Available online at www.sciencedirect.com
ScienceDirect
Journal of Sound and Vibration 311 (2008) 498–515
JOURNAL OF SOUND AND VIBRATION
www.elsevier.com/locate/jsvi

Three-dimensional vibration analysis of functionally graded material sandwich plates

Q. Li, V.P. Iu*, K.P. Kou

Department of Civil and Environmental Engineering, University of Macau, Av. Padre Tomás Pereira S.J., Taipa, Macao SAR, PR China

Received 26 January 2007; received in revised form 25 July 2007; accepted 23 September 2007
Available online 5 November 2007

Abstract

Free vibration of functionally graded material sandwich rectangular plates with simply supported and clamped edges is studied based on the three-dimensional linear theory of elasticity. Two common types of FGM sandwich plates, namely, the sandwich with FGM facesheet and homogeneous core and the sandwich with homogeneous facesheet and FGM core, are considered. The three displacements of the plates are expanded by a series of Chebyshev polynomials multiplied by appropriate functions to satisfy the essential boundary conditions. The natural frequencies are obtained by Ritz method. Rapid convergence is observed in this study. The natural frequencies of simply supported power-law FGM sandwich plates are compared with results from different two-dimensional plate theories. Parametric study is performed for varying volume fraction, layer thickness ratios, thickness–length ratios and aspect ratios of the sandwich plates.

1. Introduction

Functionally graded materials (FGMs) are a new generation of engineered materials first introduced by a group of Japanese scientists in 1984 [1,2]. The original purpose of FGMs was the development of super-resistant materials for propulsion systems and airframe of the space planes in decreasing thermal stresses and increasing the effect of protection from heat. The Japanese scientists mixed the ceramic and metal powders into a graded profile to manufacture these novel materials. The engineering ceramic can resist the severe thermal loading from the high-temperature environment; the metal is served to decrease the large tensile stress occurring on the ceramic surface at the earlier stage of cooling. Moreover, due to the special manufacturing process, these novel materials are macroscopically homogeneous in spite of microscopically inhomogeneous. The composition and structure of FGMs continuously and gradually varying over volume results in continuous and gradual changes in the properties of the material. This advantage eliminates interface problems of composite materials and thus the stress distribution becomes smooth. Used as coatings and interfacial zones, they can help to reduce mechanically and thermally induced stresses caused by the material property mismatch and to improve the bonding strength.

*Corresponding author. Tel.: +853 397 4301; fax: +853 831 694.
E-mail address: vaipaniu@umac.mo (V.P. Iu).

0022-460X/$ - see front matter © 2007 Elsevier Ltd. All rights reserved.
doi:10.1016/j.jsv.2007.09.018

Because of the wide application of FGMs, many studies have been performed to analyze the behavior and to understand the mechanics and mechanism of FGM structures. Extensive studies had been carried out, both theoretically and experimentally, on fracture mechanics [3,4], thermal stress distribution [5a,5b,6], processing [7,8], and so on. Among these FGM structures, the plates and shells are still the interests for researchers because of their applications. Approaches such as using shear deformation plate theory, energy method, and finite-element method were carried out. Reddy [9] presented the solutions of static behavior for the FGM rectangular plates based on his third-order shear deformation plate theory. Cheng and Batra [10] presented the results for the buckling and steady state vibrations of a simply supported FGM polygonal plate based on Reddy's plate theory. Loy et al. [11] presented Rayleigh–Ritz solutions for free vibration of simply supported cylindrical shells made of an FGM compound of stainless steel and nickel by using Love's shell theory. Praveen and Reddy [12] investigated the nonlinear static and dynamic response of functionally graded ceramic-metal plates using a plate finite element that accounts for the transverse shear strains, rotary inertia and moderately large rotations in the von Karman sense.

There are also several studies about finding the three-dimensional exact solutions for FGM plates. Reddy and Cheng [13] obtained a three-dimensional solution of a smart FGM plate consisting of a plate made of FGM and actuators made of an active material by the combination of the transfer matrix formulation and asymptotic expansion. Vel and Batra [14] presented a three-dimensional exact solution for free and forced vibrations of simply supported FGM rectangular plates by using suitable displacement functions to reduce equations governing steady state vibration of the plate.

The FGM sandwich can alleviate the large interfacial shear stress concentration because of the gradual variation of material properties at the facesheet–core interface. The effects of FGM core were studied by Venkataraman and Sankar [15], and Anderson [16] on the shear stresses at the facesheet–core of FGM sandwich beam. Pan and Han [17] analyzed the static response of the multilayered rectangular plate made of functionally graded, anisotropic, and linear magneto-electro-elastic materials. Das et al. [18] studied a sandwich composed of a single FGM soft core with relatively orthotropic stiff facesheets by using a triangular plate element. Shen [19] considered two types of FGM hybrid laminated plates, one is with FGM core and piezoelectric ceramic facesheet and the other is with FGM facesheet and piezoelectric ceramic core.

The FGM sandwich construction commonly exists in two types: FGM facesheet–homogeneous core and homogeneous facesheet–FGM core. For the case of homogeneous core, the softcore is commonly employed because of the light weight and high bending stiffness in the structural design. The homogeneous hardcore is also employed in other fields such as control or in the thermal environments. The actuators and sensors which are commonly piezoelectric ceramics, are always in the mid layers of the sandwich construction as in the paper of Shen [19]. Moreover, in the thermal environments, the metal-rich facesheet can reduce the large tensile stress on the surface at the early stage of cooling [20].

In general, the plates made of FGMs are not materially symmetric about the midplane for the special material properties distribution. Their stretching and flexural deformation modes are coupled. This case can be avoided for the multilayer FGM systems if the FGM constituent is positioned at the top and bottom layers. Zenkour [21a,b] had presented a two-dimensional solution for bending, buckling, and free vibration analysis of simply supported functionally graded ceramic-metal sandwich plates based on the sinusoidal shear deformation plate theory.

In the present study, the three-dimensional free vibration of multi-layer FGM system–symmetric and unsymmetric FGM sandwich plates are analyzed by Ritz method. Two common types of FGM sandwich plates, namely, the sandwich with FGM facesheet and homogeneous core and the sandwich with homogeneous facesheet and FGM core are considered. The three displacements of rectangular plates are expanded by Chebyshev polynomial series multiplied by boundary functions [22,23]. The variation of material properties through the thickness of the sandwich is expressed by employing one continuously sectional function. The present approach is validated by the comparisons of other theories and methods. The convergence study reveals the relationships between the convergence rate and volume fraction index κ value, material property distribution. The effects of κ values, material property distributions, supported conditions, thickness-side ratios and aspect ratios are also discussed in the parametric study.

2. Problem formulation

2.1. Geometrical configuration

Consider the case of a uniform thickness, rectangular FGM sandwich plate composed of three microscopically heterogeneous layers referring to a rectangular coordinates (x_1, x_2, x_3) as shown in Fig. 1. The top and bottom faces of the plate are at $x_3 = \pm h/2$, and the edges of the plate are parallel to axes x_1 and x_2. The corresponding displacement components at generic points are u_1, u_2, and u_3 in the x_1, x_2, and x_3 directions, respectively.

For coding and derivational convenience, the non-dimensional parameters are introduced

$$\xi = \frac{2x_1}{a}, \quad \eta = \frac{2x_2}{b}, \quad \zeta = \frac{2x_3}{h}, \tag{1}$$

where $\xi, \eta, \zeta \in [-1, 1]$.

The sandwich plate are composed of three elastic layers, namely, "Layer 1", "Layer 2", and "Layer 3" from bottom to top of the plate. The vertical ordinates of the bottom, the two interfaces, and the top are denoted by $h_1 = -h/2, h_2, h_3, h_4 = h/2$, respectively. For the brevity, the ratio of the thickness of each layer from bottom to top is denoted by the combination of three numbers, i.e. "1-0-1", "2-1-2" and so on. As shown in Fig. 2, two types A and B are considered in the present study:

Type A: FGM facesheet and homogeneous core
Type B: Homogeneous facesheet and FGM core

2.2. Material properties

The properties of FGM vary continuously due to gradually changing the volume fraction of the constituent materials, usually in the thickness direction only. Power-law function [24,25] are commonly used to describe

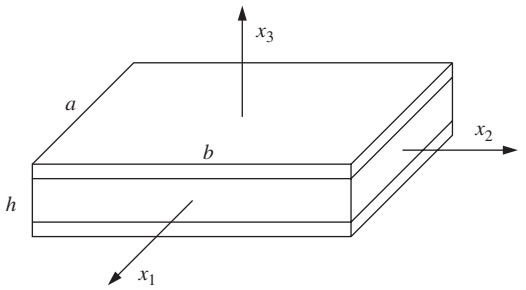

Fig. 1. Geometry of rectangular FGM sandwich plate with uniform thickness in the rectangular Cartesian coordinates.

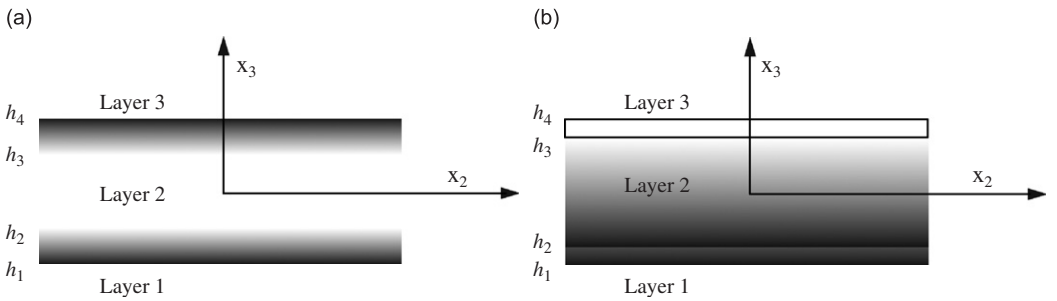

Fig. 2. The material variation along the thickness of the FGM sandwich plate: (a) FGM facesheet and homogeneous core (b) homogeneous facesheet and FGM core.

these variations of materials properties. The sandwich structure made of two types of power-law FGMs mentioned before are discussed as follows.

2.2.1. Type A: power-law FGM facesheet and homogeneous core

The volume fraction of the FGMs is assumed to obey a power-law function along the thickness direction:

$$g^{(1)}(\zeta) = \left(\frac{\zeta - \zeta_1}{\zeta_2 - \zeta_1}\right)^{\kappa}, \quad \zeta \in [\zeta_1, \zeta_2], \tag{2a}$$

$$g^{(2)}(\zeta) = 1, \quad \zeta \in [\zeta_2, \zeta_3], \tag{2b}$$

$$g^{(3)}(\zeta) = \left(\frac{\zeta - \zeta_4}{\zeta_3 - \zeta_4}\right)^{\kappa}, \quad \zeta \in [\zeta_3, \zeta_4], \tag{2c}$$

where $g^{(i)}, (i = 1, 2, 3)$ denotes the volume fraction function of layer i; $\zeta_j = 2h_j/h, (j = 1, 2, 3, 4)$; κ is the volume fraction index ($0 \leqslant \kappa \leqslant +\infty$), which dictates the material variation profile through the thickness.

2.2.2. Type B: homogeneous facesheet and power-law FGM core

The volume fraction of the FGMs is assumed to obey a power-law function along the thickness direction:

$$g^{(1)}(\zeta) = 0, \quad \zeta \in [\zeta_1, \zeta_2], \tag{3a}$$

$$g^{(2)}(\zeta) = \left(\frac{\zeta - \zeta_2}{\zeta_3 - \zeta_2}\right)^{\kappa}, \quad \zeta \in [\zeta_2, \zeta_3], \tag{3b}$$

$$g^{(3)}(\zeta) = 1, \quad \zeta \in [\zeta_3, \zeta_4] \tag{3c}$$

in which $g^{(i)}$, ζ_j and κ are as same as defined in Eq. (2).

The effective material properties, like Young's modulus E, Poisson's ratio v, and mass density ρ, then can be expressed by the rule of mixture [3] as

$$\mathscr{P}^{(i)}_{\text{eff}}(\zeta) = \mathscr{P}_2 + (\mathscr{P}_1 - \mathscr{P}_2)g^{(i)}(\zeta), \tag{4}$$

where $\mathscr{P}^{(i)}_{\text{eff}}$ is the effective material property of FGM of layer i. For type A, $\mathscr{P}_1$ and $\mathscr{P}_2$ are the properties of the top and bottom faces of layer 1, respectively, and vice versa for layer 3 depending on the volume fraction $g^{(i)}(\zeta), (i = 1, 2, 3)$; For type B, $\mathscr{P}_1$ and $\mathscr{P}_2$ are the properties of layer 3 and layer 1, respectively.

These two types of FGM sandwich plates will be discussed later in the following sections. For simplicity, Poisson's ratio of plate is assumed to be constant in this study for that the effect of Poisson's ratio on the deformation is much less than that of Young's modulus [26].

3. Solution methodology

In the case of a plate undergoing free vibration, its periodic displacement components can be expressed in terms of the displacement amplitude functions:

$$u_i(\xi, \eta, \zeta, t) = U_i(\xi, \eta, \zeta)\mathrm{e}^{\mathrm{i}\omega t} \quad (i = 1, 2, 3), \tag{5}$$

where ω denotes the natural frequency of the plate and $i = \sqrt{-1}$. In the present approach, the mechanical displacement amplitude functions $U_1(\xi, \eta, \zeta)$, $U_2(\xi, \eta, \zeta)$, and $U_3(\xi, \eta, \zeta)$ in Eq. (5) are written in the form of the triplicate series of Chebyshev polynomial:

$$U_1(\xi, \eta, \zeta) = \mathscr{R}_{u_1} \sum_{i=1}^{\infty} \sum_{j=1}^{\infty} \sum_{k=1}^{\infty} A_{ijk} P_i(\xi) P_j(\eta) P_k(\zeta),$$

$$U_2(\xi, \eta, \zeta) = \mathscr{R}_{u_2} \sum_{l=1}^{\infty} \sum_{m=1}^{\infty} \sum_{n=1}^{\infty} B_{lmn} P_l(\xi) P_m(\eta) P_n(\zeta),$$

$$U_3(\xi,\eta,\zeta) = \mathscr{R}_{u_3} \sum_{p=1}^{\infty}\sum_{q=1}^{\infty}\sum_{r=1}^{\infty} C_{pqr} P_p(\xi) P_q(\eta) P_r(\zeta), \tag{6}$$

in which $\mathscr{R}_\delta, (\delta = u_1, u_2, u_3)$ are R-functions [28] to satisfy the essential boundary conditions along the edges; A_{ijk}, B_{lmn}, and C_{pqr} are the unknown coefficients to be determined; P_i, $(i = 1, 2, 3, \ldots)$ is the one-dimensional ith Chebyshev polynomial [27] (refer to Appendix A):

$$P_i(x) = \cos[(i-1)\arccos(x)]. \tag{7}$$

Chebyshev polynomials $P_i(x)$ are a set of complete and orthogonal function in the interval $[-1, 1]$. In Zhou's analysis of plates [22,23], these polynomials showed some advantages such as high convergence rate and stability. In the present approach, the three displacement components of the plates are expanded by the triplicate series of Chebyshev polynomials multiplied by the boundary functions. The thickness expansion in Chebyshev polynomials resembles the kinematical assumption of displacements in the thickness coordinate in the two-dimensional plate theories which include classical plate theory (CPT), first-order shear deformation plate theory (FSDT), third-order shear deformation plate theory (TSDT) and sinusoidal shear deformation plate theory (SSDT) as shown in Table 1.

For Ritz method, the natural boundary conditions for simply supported and clamped plates considered in the present study are

$$\begin{aligned} &u_2 = u_3 = 0, \quad \text{at } x_1 = \pm a/2 \\ &u_1 = u_3 = 0, \quad \text{at } x_2 = \pm b/2 \end{aligned} \quad \text{for simply supported condition;} \tag{8a}$$

$$\begin{aligned} &u_1 = u_2 = u_3 = 0, \quad \text{at } x_1 = \pm a/2 \\ &u_1 = u_2 = u_3 = 0, \quad \text{at } x_2 = \pm b/2 \end{aligned} \quad \text{for clamped condition.} \tag{8b}$$

The corresponding R-functions of these two boundary conditions are tabulated in Table 2.

The Hamilton's principle has the form

$$\delta \int_{t_0}^{t_1} L \,\mathrm{d}t = \delta \int_{t_0}^{t_1} (T - U + W)\,\mathrm{d}t = 0, \tag{9}$$

where $L = T - U + W$ is the Lagrangian function; T is the total kinetic energy; U is the strain energy; W is the work done by the external forces. In the case of free vibration, the principle Eq. (9) is reduced by setting the virtual work W zero. The kinetic energy in the present case is

$$T = \int_V \frac{1}{2}\rho(\zeta)\left[\left(\frac{\partial u_1}{\partial t}\right)^2 + \left(\frac{\partial u_2}{\partial t}\right)^2 + \left(\frac{\partial u_3}{\partial t}\right)^2\right]\mathrm{d}V, \tag{10}$$

Table 1
Kinematical assumptions of different plate theories

Theories	Assumption of three-dimensional displacements $u_i, i = 1, 2$ and u_3
CPT	$u_i(x_1, x_2, x_3, t) = \bar{u}_i(x_1, x_2, t) - x_3 \dfrac{\partial w}{\partial x_i}$,
	$u_3(x_1, x_2, x_3, t) = w(x_1, x_2, t)$
FSDT	$u_i(x_1, x_2, x_3, t) = \bar{u}_i(x_1, x_2, t) + x_3 \phi_{x_i}(x_1, x_2, t)$,
	$u_3(x_1, x_2, x_3, t) = w(x_1, x_2, t)$
TSDT	$u_i(x_1, x_2, x_3, t) = \bar{u}_i(x_1, x_2, t) + x_3 \phi_{x_i}(x_1, x_2, t) - \dfrac{4x_3^3}{3h^2}\left(\phi_{x_i} + \dfrac{\partial w}{\partial x_i}\right)$,
	$u_3(x_1, x_2, x_3, t) = w(x_1, x_2, t)$
SSDT	$u_i(x_1, x_2, x_3, t) = \bar{u}_i(x_1, x_2, t) - x_3 \dfrac{\partial w}{\partial x_i} + \dfrac{h}{\pi}\sin\left(\dfrac{\pi x_3}{h}\right)\phi_{x_i}(x_1, x_2, t)$
	$u_3(x_1, x_2, x_3, t) = w(x_1, x_2, t)$

Table 2
Boundary R-functions for different boundary conditions

BC	R-functions
Simply supported	$\mathscr{R}_{u_1} = 1-\eta^2$, $\mathscr{R}_{u_2} = 1-\xi^2$, $\mathscr{R}_{u_3} = (1-\xi^2)(1-\eta^2)$
Clamped	$\mathscr{R}_{u_1} = \mathscr{R}_{u_2} = \mathscr{R}_{u_3} = (1-\xi^2)(1-\eta^2)$

where $\rho(\zeta)$ is the effective thickness-graded mass density defined by Eq. (4). The linear elastic strain energy U is written in integral form as

$$U = \int_V \frac{E(\zeta)}{2(1+\nu)}\left(\frac{\nu}{1-2\nu}\Upsilon_1^2 + \Upsilon_2 + \frac{\Upsilon_3}{2}\right) \mathrm{d}V, \tag{11}$$

where $E(\zeta)$ is the effective thickness-graded Young's modulus defined by Eq. (4) and

$$\Upsilon_1 = \frac{\partial u_1}{\partial x_1} + \frac{\partial u_2}{\partial x_2} + \frac{\partial u_3}{\partial x_3}, \quad \Upsilon_2 = \left(\frac{\partial u_1}{\partial x_1}\right)^2 + \left(\frac{\partial u_2}{\partial x_2}\right)^2 + \left(\frac{\partial u_3}{\partial x_3}\right)^2,$$

$$\Upsilon_3 = \left(\frac{\partial u_1}{\partial x_2} + \frac{\partial u_2}{\partial x_1}\right)^2 + \left(\frac{\partial u_2}{\partial x_3} + \frac{\partial u_3}{\partial x_2}\right)^2 + \left(\frac{\partial u_1}{\partial x_3} + \frac{\partial u_3}{\partial x_1}\right)^2. \tag{12}$$

By Ritz method, the variation of Lagrangian function L should equal zero under the integration with respect to time carried out between fixed initial and final instants of time t_0 and t_1. The Lagrangian function L is a homogeneous quadratic function of Chebyshev polynomial series coefficients. Its partial differential with respect to coefficients A_{ijk}, B_{lmn}, and C_{pqr}

$$\frac{\partial L}{\partial A_{ijk}} = 0, \quad \frac{\partial L}{\partial B_{lmn}} = 0, \quad \frac{\partial L}{\partial C_{pqr}} = 0 \quad (i,j,k,l,m,n,p,q,r = 1,2,3,\ldots) \tag{13}$$

leads to the governing eigenvalue matrix:

$$\left(\begin{bmatrix} \mathbf{K}_{11} & \mathbf{K}_{12} & \mathbf{K}_{13} \\ \mathbf{K}_{12}^{\mathrm{T}} & \mathbf{K}_{22} & \mathbf{K}_{23} \\ \mathbf{K}_{13}^{\mathrm{T}} & \mathbf{K}_{23}^{T} & \mathbf{K}_{33} \end{bmatrix} - \omega^2 \begin{bmatrix} \mathbf{M}_{11} & 0 & 0 \\ 0 & \mathbf{M}_{22} & 0 \\ 0 & 0 & \mathbf{M}_{33} \end{bmatrix}\right) \begin{Bmatrix} \mathbf{A} \\ \mathbf{B} \\ \mathbf{C} \end{Bmatrix} = 0, \tag{14}$$

where **A**, **B**, and **C** are the column vectors containing unknown coefficients, A_{ijk}, B_{lmn}, and C_{pqr}, respectively. The explicit forms of the respective elements in the nominal stiffness matrix **K** and mass matrix **M** are listed in Appendix B.

4. Numerical results

4.1. Convergence and efficiency study

Theoretically, the Ritz method can provide accurate solutions. The accuracy and efficiency of solutions depend greatly on the choice of displacement components amplitude functions U_i. The natural frequencies obtained in the present approach start with an initial value and converge. These initial estimates can be improved by increasing the number of terms of admissible functions in the computation. In fact, the convergence rate is very high and is independent of the volume fraction indices κ values [29]. In the present study, the square power-law FGM sandwich plates with four simply supported and clamped edges are taken as examples for the convergence study.

Considering an FGM plate of Type A as shown in Fig. 2(a), the Young's modulus and mass density of layer 1 are $E_c = 380\,\mathrm{GPa}$ and $\rho_c = 3800\,\mathrm{kg/m^3}$ ($\mathscr{P}_1$, alumina) at the top face and $E_m = 70\,\mathrm{GPa}$ and

$\rho_m = 2707\,kg/m^3$ ($\mathscr{P}_2$, aluminum) at the bottom face. And the Young's modulus and mass density between these two faces vary according to the power-law. Poisson's ratio v is taken as 0.3 throughout the analyses.

For simplicity, the non-dimensional natural frequency parameter is defined as

$$\bar{\omega} = \frac{\omega b^2}{h}\sqrt{\frac{\rho_0}{E_0}}, \tag{15}$$

where $\rho_0 = 1\,kg/m^3$, $E_0 = 1\,GPa$.

Due to the symmetry of the plate and the boundary conditions, the vibrational modes can be classified into symmetric modes and antisymmetric modes. These two modes can be determined separately and resulted in a smaller set of eigenvalue equations while maintaining the same level of accuracy. For the completeness, the expansions in ξ and η directions consist of the complete set of series; whereas the expansions in ζ direction consist of the antisymmetric terms only.

Tables 3 and 4 show the convergence of flexural vibration frequency parameter $\bar{\omega}$ of square 2-1-2 power-law FGM plates of Type A (FGM facesheet and homogeneous core) with volume fraction index κ values ($\kappa = 1, 10$) and two thickness ratios ($h/b = 0.01, 0.1$). It can be seen that the frequencies converge with the increase in the number of terms of admissible functions. This number of terms of admissible function is a combination of the number of the thickness expansion terms and the number of the length and width sides expansions terms, which depend on the thickness and boundary conditions, respectively. Tables 5 and 6 show the convergence of square power-law FGM plate of Type B (homogeneous facesheet and FGM core), of which the material distribution is chosen as 1-8-1 same with $\kappa = 1, 10$ and $h/b = 0.01, 0.1$. They have the same trend as the case of 2-1-2 power-law FGM plates of Type A. For both thickness-side ratios ($h/b = 0.01, 0.1$), two terms of thickness expansion are sufficient regardless of the boundary conditions (simply supported or clamped) and the volume fraction index values ($\kappa = 1, 10$). And totally $10 \times 10 \times 2$ terms can provide the accurate enough solutions as compared with solutions of $12 \times 12 \times 3$ or $12 \times 12 \times 4$ terms.

Table 3
Convergence of flexural vibration frequency parameters $\bar{\omega}$ of square 2-1-2 power-law FGM plates with $\kappa = 1$ ($h/b = 0.01, 0.1$)

h/b	Terms	$\bar{\omega}_1$	$\bar{\omega}_2$	$\bar{\omega}_3$	$\bar{\omega}_4$	$\bar{\omega}_5$
0.01	Simply supported					
	$10 \times 10 \times 1$	1.47169	3.67778	3.67778	5.88214	7.35076
	$10 \times 10 \times 2$	1.32974	3.32324	3.32324	5.31543	6.64283
	$11 \times 11 \times 1$	1.47169	3.67778	3.67778	5.88214	7.35076
	$11 \times 11 \times 2$	1.32974	3.32324	3.32324	5.31543	6.64283
	$12 \times 12 \times 3$	1.32974	3.32324	3.32324	5.31543	6.64282
	Clamped					
	$10\times10 \times 1$	2.68146	5.46547	5.46547	8.05363	9.78950
	$10\times10 \times 2$	2.43753	4.96512	4.96512	7.31581	8.90241
	$10\times10 \times 3$	2.43752	4.96511	4.96511	7.31579	8.90238
	$11\times11 \times 2$	2.43347	4.96340	4.96340	7.31565	8.88625
	$12\times12 \times 3$	2.43342	4.95815	4.95815	7.30599	8.88603
0.1	Simply supported					
	$10 \times 10 \times 1$	1.43532	3.46523	3.46523	5.37039	6.58110
	$10 \times 10 \times 2$	1.30186	3.15897	3.15897	4.91713	6.04132
	$10 \times 10 \times 3$	1.30182	3.15875	3.15875	4.91660	6.04051
	$11 \times 11 \times 3$	1.30182	3.15875	3.15875	4.91660	6.04051
	$12 \times 12 \times 4$	1.30182	3.15875	3.15875	4.91659	6.04048
	Clamped					
	$10\times10 \times 1$	2.49612	4.83861	4.83861	6.84852	8.13006
	$10\times10 \times 2$	2.29302	4.47175	4.47175	6.35688	7.56849
	$10\times10 \times 3$	2.29260	4.47053	4.47053	6.35478	7.56564
	$11\times11 \times 3$	2.29108	4.46888	4.46888	6.35280	7.56182
	$12\times12 \times 4$	2.29049	4.46721	4.46721	6.35053	7.56005

Table 4
Convergence of flexural vibration frequency parameters $\bar{\omega}$ of square 2-1-2 power-law FGM plates with $\kappa = 10$ ($h/b = 0.01, 0.1$)

h/b	Terms	$\bar{\omega}_1$	$\bar{\omega}_2$	$\bar{\omega}_3$	$\bar{\omega}_4$	$\bar{\omega}_5$
0.01	Simply supported					
	10×10 × 1	1.06179	2.65359	2.65359	4.24435	5.30429
	10×10 × 2	0.95937	2.39777	2.39777	3.83540	4.79339
	10×10 × 3	0.95935	2.39763	2.39763	3.83505	4.79284
	11×11 × 2	0.95937	2.39777	2.39777	3.83540	4.79339
	12×12 × 3	0.95935	2.39763	2.39763	3.83505	4.79283
	Clamped					
	10×10 × 1	1.93484	3.94414	3.94414	5.81255	7.06575
	10×10 × 2	1.75883	3.58303	3.58303	5.27993	6.42541
	10×10 × 3	1.75867	3.58249	3.58249	5.27884	6.42384
	11×11 × 2	1.75589	3.58180	3.58180	5.27987	6.41367
	12×12 × 3	1.75571	3.57747	3.57747	5.27176	6.41203
0.1	Simply supported					
	10×10 × 1	1.03968	2.52326	2.52326	3.92820	4.82671
	10×10 × 2	0.94283	2.29954	2.29954	3.59555	4.42964
	10×10 × 3	0.94078	2.28808	2.28808	3.56911	4.39095
	11×11 × 3	0.94078	2.28808	2.28808	3.56911	4.39095
	12×12 × 4	0.94044	2.28616	2.28616	3.56466	4.38441
	Clamped					
	10×10 × 1	1.82541	3.56617	3.56617	5.07402	6.04522
	10×10 × 2	1.67635	3.29431	3.29431	4.70829	5.62707
	10×10 × 3	1.66421	3.25798	3.25798	4.64478	5.54034
	11×11 × 3	1.66326	3.25650	3.25650	4.64271	5.53778
	12×12 × 4	1.66075	3.24938	3.24938	4.63070	5.52175

Table 5
Convergence of flexural vibration frequency parameters $\bar{\omega}$ of square 1-8-1 power-law FGM plates of Type B with $\kappa = 1$, ($h/b = 0.01, 0.1$)

h/b	Terms	$\bar{\omega}_1$	$\bar{\omega}_2$	$\bar{\omega}_3$	$\bar{\omega}_4$	$\bar{\omega}_5$
0.01	Simply supported					
	10 × 10 × 1	1.74429	4.35823	4.35823	6.96918	8.70817
	10 × 10 × 2	1.57601	3.93789	3.93789	6.29722	7.86869
	11 × 11 × 1	1.74429	4.35823	4.35823	6.96918	8.70817
	11 × 11 × 2	1.57601	3.93789	3.93789	6.29722	7.86869
	12 × 12 × 3	1.57601	3.93787	3.93787	6.29717	7.86861
	Clamped					
	10×10 × 1	3.17714	6.47370	6.47370	9.53637	11.59013
	10×10 × 2	2.88787	5.88032	5.88032	8.66126	10.53745
	10×10 × 3	2.88784	5.88025	5.88025	8.66110	10.53723
	11×11 × 2	2.88311	5.87820	5.87821	8.66082	10.51868
	12×12 × 3	2.88298	5.87200	5.87200	8.64946	10.51798
0.1	Simply supported					
	10 × 10 × 1	1.68255	4.00585	4.00585	6.13700	7.47037
	10 × 10 × 2	1.52306	3.63486	3.63486	5.58000	6.80058
	10 × 10 × 3	1.52276	3.63314	3.63314	5.57586	6.79435
	11 × 11 × 3	1.52276	3.63314	3.63314	5.57586	6.79435
	12 × 12 × 4	1.52208	3.62953	3.62953	5.56787	6.78289
	Clamped					
	10×10 × 1	2.86053	5.44192	5.44192	7.61270	8.96085
	10×10 × 2	2.61320	4.98420	4.98420	6.98593	8.23134
	10×10 × 3	2.61069	4.97654	4.97654	6.97266	8.21368
	11×11 × 3	2.60914	4.97440	4.97440	6.96982	8.21051
	12×12 × 4	2.60503	4.96303	4.96303	6.95161	8.18719

Table 6
Convergence of flexural vibration frequency parameters $\bar{\omega}$ of square 1-8-1 power-law FGM plates of Type B with $\kappa = 10$ ($h/b = 0.01, 0.1$)

h/b	Terms	$\bar{\omega}_1$	$\bar{\omega}_2$	$\bar{\omega}_3$	$\bar{\omega}_4$	$\bar{\omega}_5$
0.01	Simply supported					
	10×10 × 1	1.72383	4.30750	4.30750	6.88871	8.60815
	10×10 × 2	1.55756	3.89229	3.89229	6.22508	7.77922
	10×10 × 3	1.55755	3.89220	3.89220	6.22485	7.77886
	11×11 × 2	1.55756	3.89229	3.89229	6.22508	7.77922
	12×12 × 3	1.55755	3.89220	3.89220	6.22485	7.77885
	Clamped					
	10×10 × 1	3.14039	6.39988	6.39988	9.42913	11.46067
	10×10 × 2	2.85474	5.81414	5.81414	8.56560	10.42242
	10×10 × 3	2.85464	5.81379	5.81379	8.56490	10.42141
	11×11 × 2	2.85000	5.81210	5.81210	8.56534	10.40363
	12×12 × 3	2.84983	5.80565	5.80565	8.55342	10.40233
0.1	Simply supported					
	10×10 × 1	1.67228	4.00978	4.00978	6.17880	7.54643
	10×10 × 2	1.51706	3.65652	3.65652	5.65925	6.92978
	10×10 × 3	1.51576	3.64938	3.64938	5.64295	6.90604
	11×11 × 3	1.51576	3.64938	3.64938	5.64295	6.90604
	12×12 × 4	1.51523	3.64651	3.64651	5.63646	6.89665
	Clamped					
	10×10 × 1	2.87593	5.52262	5.52262	7.76954	9.18391
	10×10 × 2	2.64451	5.10939	5.10939	7.21810	8.55574
	10×10 × 3	2.63661	5.08632	5.08632	7.17872	8.50223
	11×11 × 3	2.63515	5.08405	5.08405	7.17553	8.49926
	12×12 × 4	2.63156	5.07426	5.07426	7.15975	8.47828

Table 7
Comparisons of fundamental frequency parameters $\omega^* = \omega a^2/(2\pi)\sqrt{\rho h/D}$ of a simply supported isotropic rectangular plates with other theories ($b = 2a$)

h/b	0.005	0.01	0.02	0.1	0.2
CPT	1.96339	1.96309	1.96188	1.92433	1.81954
FSDT	1.96305	1.96171	1.95639	1.80958	1.51101
$N = 1$	1.96311	1.96196	1.95727	1.82785	1.56003
TSDT	1.96305	1.96171	1.95639	1.80974	1.51230
SSDT	1.96305	1.96171	1.95640	1.80993	1.51294
$N = 2$	1.96305	1.96178	1.95662	1.81524	1.53201
DQM	1.96299	1.96179	1.95667	1.81513	1.53118
$N = 3$	1.96305	1.96178	1.95662	1.81513	1.53112

4.2. Verification

The numerical results of simply supported rectangular isotropic plates and power-law FGM plates are verified in this subsection.

The numerical results of frequency parameters of the first flexural mode of simply supported rectangular isotropic plates are compared with the results of CPT, FSDT, TSDT, SSDT, and differential quadrature method (DQM) [30] in Table 7. For flexural vibration, only the antisymmetric terms ($i = 2, 4, 6, \ldots$ in Eq. (7)) are needed along the thickness direction ζ in the expansions of u_1 and u_2. N denotes the number of the antisymmetric terms of u_1 and u_2 in the thickness directions. For thin plates, the present approach almost gives the identical results as other approaches.

Table 8
Comparisons of natural fundamental frequency parameters $\bar{\omega}$ of simply supported square power-law FGM plates of Type A with other theories ($h/b = 0.1$)

κ	Method	1-0-1	2-1-2	2-1-1	1-1-1	2-2-1	1-2-1
0.5	CPT	1.47157	1.51242	1.54264	1.54903	1.58374	1.60722
	FSDT	1.44168	1.48159	1.51035	1.51695	1.55001	1.57274
	TSDT	1.44424	1.48408	1.51253	1.51922	1.55199	1.57451
	SSDT	1.44436	1.48418	1.51258	1.51927	1.55202	1.57450
	Present	1.44614	1.48608	1.50841	1.52131	1.54926	1.57668
1	CPT	1.26238	1.32023	1.37150	1.37521	1.43247	1.46497
	FSDT	1.24031	1.29729	1.34637	1.35072	1.40555	1.43722
	TSDT	1.24320	1.30011	1.34888	1.35333	1.40789	1.43934
	SSDT	1.24335	1.30023	1.34894	1.35339	1.40792	1.43931
	Present	1.24470	1.30181	1.33511	1.35523	1.39763	1.44137
5	CPT	0.95844	0.99190	1.08797	1.05565	1.16195	1.18867
	FSDT	0.94256	0.97870	1.07156	1.04183	1.14467	1.17159
	TSDT	0.94598	0.98184	1.07432	1.04466	1.14731	1.17397
	SSDT	0.94630	0.98207	1.07445	1.04481	1.14741	1.17399
	Present	0.94476	0.98103	1.02942	1.04532	1.10983	1.17567
10	CPT	0.94321	0.95244	1.05185	1.00524	1.11883	1.13614
	FSDT	0.92508	0.93962	1.03580	0.99256	1.10261	1.12067
	TSDT	0.92839	0.94297	1.03862	0.99551	1.10533	1.12314
	SSDT	0.92875	0.94332	1.04558	0.99519	1.04154	1.13460
	Present	0.92727	0.94078	0.98929	0.99523	1.06104	1.12466

For thick plates, the 2-D theories cannot provide the results as accurate as 3-D approaches (present approach and DQM) because 3-D approaches do not rely on any hypothesis compared with 2-D theories. The results of the present approach are close to the solutions of DQM which are numerical solutions of the 3-D governing partial differential equations. It should be noted that the results of $N = 1$ were close to the solutions of FSDT.

The results of the power-law FGM sandwich plates of Type A with six material distributions are compared in Table 8 with the results based on CPT, FSDT, TSDT, SSDT. Young's modulus E and mass density ρ are based on the power-law distribution, Eq. (4). Table 8 shows a good agreement by comparisons of FGM plates of four different volume fraction indices $\kappa = 0.5, 1, 5, 10$ with other theories.

5. Results and discussion

Based on the procedures and analyses of foregoing sections, the two types of square power-law FGM plates with four simply supported edges and four clamped edges are investigated. In the succedent computation, $10 \times 10 \times 3$ terms of admissible functions for each displacement function are used. Six-layer thickness ratios (1-0-1, 2-1-2, 1-1-1, 2-2-1, 1-2-1, 1-8-1) are selected for the analysis. Tables 9–14 give the fundamental frequency parameters $\bar{\omega}$ of these selected plates.

The numerical results of simply supported and clamped square power-law FGM plates of Type A are tabulated in Tables 9–12. Tables 9 and 10 consider the case of homogeneous hardcore in which the Young's modulus and mass density of layer 1 are $E_c = 380\,\text{GPa}$ and $\rho_c = 3800\,\text{kg/m}^3$ ($\mathscr{P}_1$, alumina) at the top face and $E_m = 70\,\text{GPa}$ and $\rho_m = 2707\,\text{kg/m}^3$ ($\mathscr{P}_2$, aluminum) at the bottom face. Tables 11 and 12 consider the case of homogeneous softcore in which the Young's modulus and mass density of layer 1 are $E_m = 70\,\text{GPa}$ and $\rho_m = 2707\,\text{kg/m}^3$ ($\mathscr{P}_1$, aluminum) at the top face and $E_c = 380\,\text{GPa}$ and $\rho_c = 3800\,\text{kg/m}^3$ ($\mathscr{P}_2$, alumina) at the bottom face. Three thickness-side ratios h/b (0.01, 0.1, 0.2) and five volume fraction indices $\kappa(0, 0.5, 1, 5, 10)$ are considered.

Table 9
Fundamental frequency parameters $\bar{\omega}$ of simply supported square power-law FGM sandwich plates with homogeneous hardcore

h/b	κ	1-0-1	2-1-2	1-1-1	2-2-1	1-2-1	1-8-1
0.01	0	1.88829	1.88829	1.88829	1.88829	1.88829	1.88829
	0.5	1.48244	1.52355	1.56046	1.59031	1.61915	1.76357
	1	1.27158	1.32974	1.38511	1.42992	1.47558	1.69906
	5	0.96563	0.99903	1.06309	1.13020	1.19699	1.56988
	10	0.95042	0.95934	1.01237	1.08065	1.14408	1.54164
0.1	0	1.82682	1.82682	1.82682	1.82682	1.82682	1.82682
	0.5	1.44614	1.48608	1.52131	1.54926	1.57668	1.71130
	1	1.24470	1.30181	1.35523	1.39763	1.44137	1.65113
	5	0.94476	0.98103	1.04532	1.10983	1.17567	1.52993
	10	0.92727	0.94078	0.99523	1.06104	1.12466	1.50333
0.2	0	1.67711	1.67711	1.67711	1.67711	1.67711	1.67711
	0.5	1.35358	1.39053	1.42178	1.44535	1.46940	1.58186
	1	1.17485	1.22915	1.27770	1.31434	1.35341	1.53142
	5	0.89086	0.93362	0.99798	1.05607	1.11900	1.42845
	10	0.86833	0.89228	0.94984	1.00949	1.07290	1.40568

Table 10
Fundamental frequency parameters $\bar{\omega}$ of clamped square power-law FGM sandwich plates with homogeneous hardcore

h/b	κ	1-0-1	2-1-2	1-1-1	2-2-1	1-2-1	1-8-1
0.01	0	3.45447	3.45447	3.45447	3.45447	3.45447	3.45447
	0.5	2.71263	2.78786	2.85535	2.90993	2.96675	3.23192
	1	2.32703	2.43347	2.53476	2.61669	2.71273	3.11384
	5	1.76711	1.82843	1.94575	2.06851	2.25938	2.87731
	10	1.73916	1.75573	1.85287	1.97781	2.09743	2.82561
0.1	0	3.13799	3.13799	3.13799	3.13799	3.13799	3.13799
	0.5	2.52593	2.59490	2.65356	2.69828	2.74989	2.95839
	1	2.19019	2.29107	2.38186	2.45108	2.53978	2.86255
	5	1.66187	1.73925	1.85790	1.96719	2.15715	2.66739
	10	1.62117	1.66326	1.76860	1.88080	1.99860	2.62431
0.2	0	2.57552	2.57552	2.57552	2.57552	2.57552	2.57552
	0.5	2.15683	2.21438	2.25866	2.28822	2.33060	2.46042
	1	1.90590	1.99492	2.06686	2.11525	2.19019	2.39709
	5	1.44469	1.54542	1.66225	1.74700	1.93215	2.26481
	10	1.38683	1.46709	1.58209	1.67158	1.78269	2.23526

Tables 13 and 14 give the results of 1-8-1 power-law FGM plate of Type B. $\mathscr{P}_1$ is referred to the properties of aluminum and $\mathscr{P}_2$ the properties of alumina. In this case, the FGM core is metal-rich at the top face and ceramic-rich at the bottom face. Three thickness-side ratios h/b (0.01, 0.1, 0.2) and five volume fraction indices κ (0.5, 1, 2, 5, 10) are considered.

It is shown that for both simply supported and clamped plates, the natural fundamental frequencies decrease with the decrease of the material rigidity, which is due to the increase of κ for Type A or the decrease of κ for Type B and the variation of the layer thickness ratios. Moreover, the thin plates are slightly more sensitive than the thick plate to material rigidity, i.e. κ, and this effect is a little greater for simply supported plates as compared with clamped plates.

Fig. 3 depicts the fundamental frequencies parameters versus the thickness-side ratios of simply supported power-law FGM sandwich plates with homogeneous hardcore. The bottom and top curves are the cases of

Table 11
Fundamental frequency parameters $\bar{\omega}$ of simply supported square power-law FGM sandwich plates with homogeneous softcore

h/b	κ	1-0-1	2-1-2	1-1-1	2-2-1	1-2-1	1-8-1
0.01	0	0.96022	0.96022	0.96022	0.96022	0.96022	0.96022
	0.5	1.66281	1.62291	1.58171	1.52277	1.50658	1.26557
	1	1.82031	1.79163	1.75379	1.68184	1.67490	1.38331
	5	1.92090	1.94313	1.93623	1.86207	1.88530	1.57035
	10	1.91064	1.94687	1.95044	1.88042	1.91162	1.60457
0.1	0	0.92897	0.92897	0.92897	0.92897	0.92897	0.92897
	0.5	1.57352	1.52588	1.48459	1.43419	1.41662	1.20553
	1	1.72227	1.67437	1.63053	1.57037	1.55788	1.30825
	5	1.84198	1.82611	1.78956	1.72726	1.72670	1.46647
	10	1.84020	1.83987	1.80813	1.74779	1.74811	1.49481
0.2	0	0.85286	0.85286	0.85286	0.85286	0.85286	0.85286
	0.5	1.37894	1.32061	1.28053	1.24533	1.22580	1.07016
	1	1.50896	1.43325	1.38242	1.34203	1.32129	1.14451
	5	1.65868	1.58011	1.50284	1.46009	1.42665	1.25210
	10	1.67278	1.60909	1.52671	1.48306	1.44101	1.27065

Table 12
Fundamental frequency parameters $\bar{\omega}$ of clamped square power-law FGM sandwich plates with homogeneous softcore

h/b	κ	1-0-1	2-1-2	1-1-1	2-2-1	1-2-1	1-8-1
0.01	0	1.75955	1.75955	1.75955	1.75955	1.75955	1.75955
	0.5	3.04486	2.97115	2.89556	2.78801	2.75819	2.31796
	1	3.33323	3.27936	3.20956	3.07834	3.06523	2.53302
	5	3.51895	3.55732	3.54268	3.40745	3.44842	2.87430
	10	3.50064	3.56482	3.56905	3.44126	3.49638	2.93670
0.1	0	1.59667	1.59667	1.59667	1.59667	1.59667	1.59667
	0.5	2.59854	2.49325	2.41822	2.34967	2.31267	2.01124
	1	2.84447	2.71205	2.61914	2.53960	2.50113	2.15476
	5	3.11435	2.98733	2.85602	2.77151	2.71561	2.36494
	10	3.13632	3.03681	2.89948	2.81400	2.74524	2.40157
0.2	0	1.31009	1.31009	1.31009	1.31009	1.31009	1.31009
	0.5	1.97334	1.85983	1.79320	1.75870	1.71847	1.55058
	1	2.16230	1.99824	1.90331	1.86427	1.81125	1.62189
	5	2.47224	2.24288	2.06578	2.02006	1.91607	1.71750
	10	2.52896	2.31381	2.11413	2.06384	1.93580	1.73394

Table 13
Fundamental frequency parameters $\bar{\omega}$ of simply supported square 1-8-1 power-law FGM sandwich plates with FGM core

h/b	κ				
	0.5	1	2	5	10
0.01	1.33931	1.38669	1.44491	1.53143	1.59105
0.1	1.29751	1.34847	1.40828	1.49309	1.54980
0.2	1.19580	1.25338	1.31569	1.39567	1.44540

Table 14
Fundamental frequency parameters $\bar{\omega}$ of clamped square 1-8-1 power-law FGM sandwich plates with FGM core

h/b	κ				
	0.5	1	2	5	10
0.01	2.45438	2.54149	2.64835	2.80692	2.91611
0.1	2.24154	2.34606	2.45973	2.60760	2.70070
0.2	1.86081	1.97993	2.09554	2.22142	2.28896

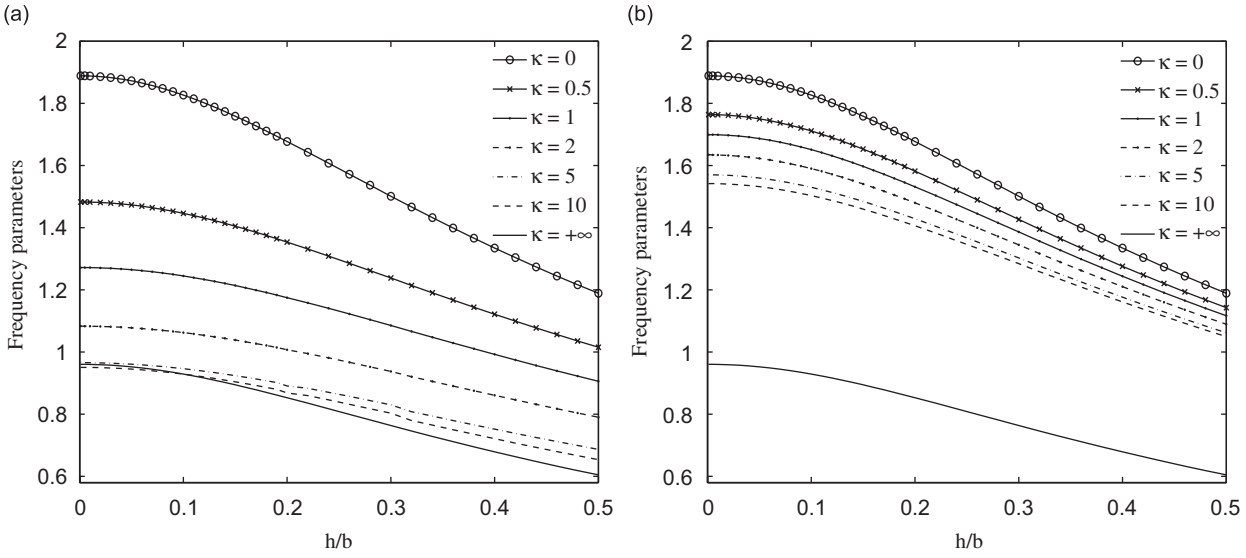

Fig. 3. Fundamental frequencies $\bar{\omega}$ for power-law FGM sandwich plates with homogeneous hardcore and four simply supported edges: (a) 1-0-1 P-FGM sandwich plate, (b) 1-8-1 P-FGM sandwich plate.

metal ($\kappa = +\infty$) and ceramic ($\kappa = 0$) plates, respectively. Fig. 4 depicts the curves of the power-law FGM sandwich plates with homogeneous softcore. The bottom and top curves are the cases of metal ($\kappa = 0$) and ceramic ($\kappa = +\infty$) plates, respectively.

It is seen that the frequencies increase with the increasing amount of ceramic in the sandwich plate. It is also shown that the effect of κ on 1-0-1 sandwich plate which is without the homogeneous core layer is greater than that of 1-8-1 sandwich with homogeneous hardcore, and the effect of κ on the sandwich with homogeneous hardcore is greater than that with homogeneous softcore.

Figs. 5 and 6 display the relative displacements along the thickness direction of the first six modes, which can be classified into two groups: flexural modes (F) and extensional modes (TE). The plate is of simply supported square 2-1-2 power-law FGM with $\kappa = 10$ and $h/b = 0.2$. These curves are the amplitudes of u_1, u_2, and u_3 of the lines ($\xi = 0, \eta = 0$) and ($\xi = 0.5, \eta = 0.5$).

For the flexural modes (F) as shown, the displacement U_3 is not uniform which implied that there is normal stress existing in the thickness direction. For F_2 and F_3 modes, the deflected plate retains the same thickness at ($\xi = 0, \eta = 0$), however, the thickness is compressed at other positions such as ($\xi = 0.5, \eta = 0.5$) with a decreasing slope of the originally normal lines. It also shows that the deformed lines, u_1 and u_2 across the thickness of the plate are not simply linear. In fact, in the process of computation, the displacement amplitude functions U_1 and U_2 are resembled by not only the constant and linear terms of the polynomials but also the higher-order terms. For the extensional modes (TE), the whole deflected plate retains the same thickness but the displacement components u_1 and u_2 are symmetrical about the mid-plane, i.e. shown in Figs. 5(d) and (e).

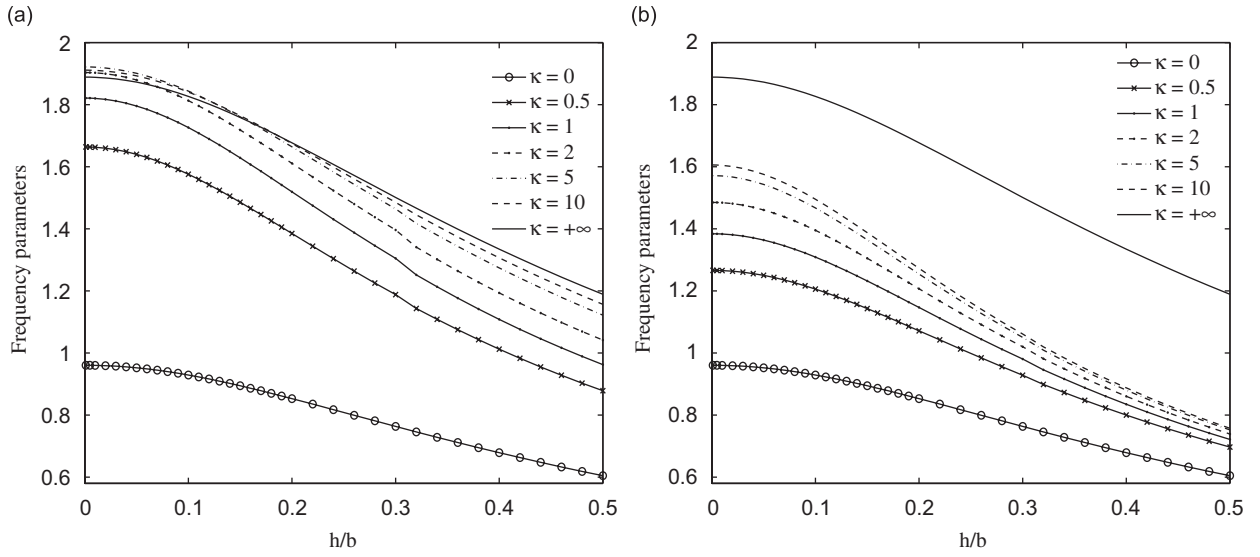

Fig. 4. Fundamental frequencies $\bar{\omega}$ for power-law FGM sandwich plates with homogeneous softcore and four simply supported edges: (a) 1-0-1 P-FGM sandwich plate, (b) 1-8-1 P-FGM sandwich plate.

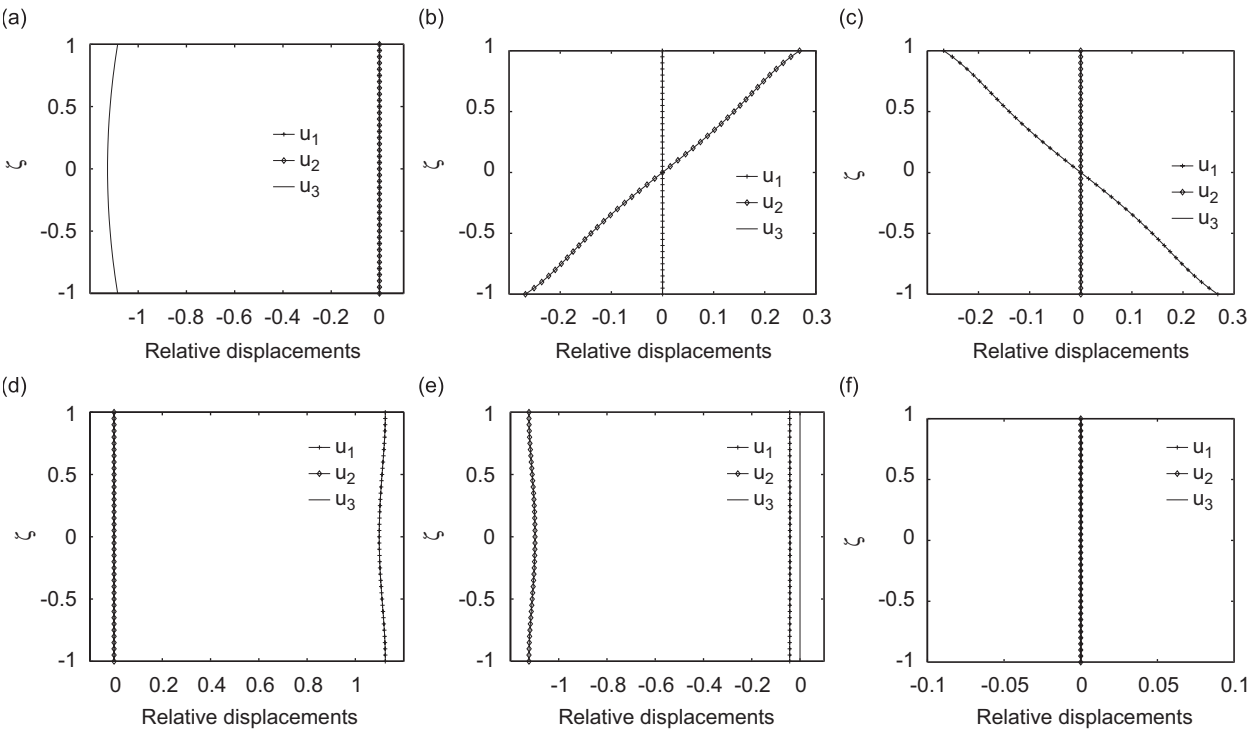

Fig. 5. Deflected shapes $U_i(0,0,\zeta), i = 1,2,3$ of the first six modes for the square plates with four simply supported edges: (a) F_1, (b) F_2, (c) F_3, (d) TE_1, (e) TE_2 and (f) F_4.

6. Conclusion

Three-dimensional vibration analysis of rectangular FGM sandwich plates has been carried out based on the linear, small strain 3-D elasticity theory via Ritz method. The present approach can provide accurate

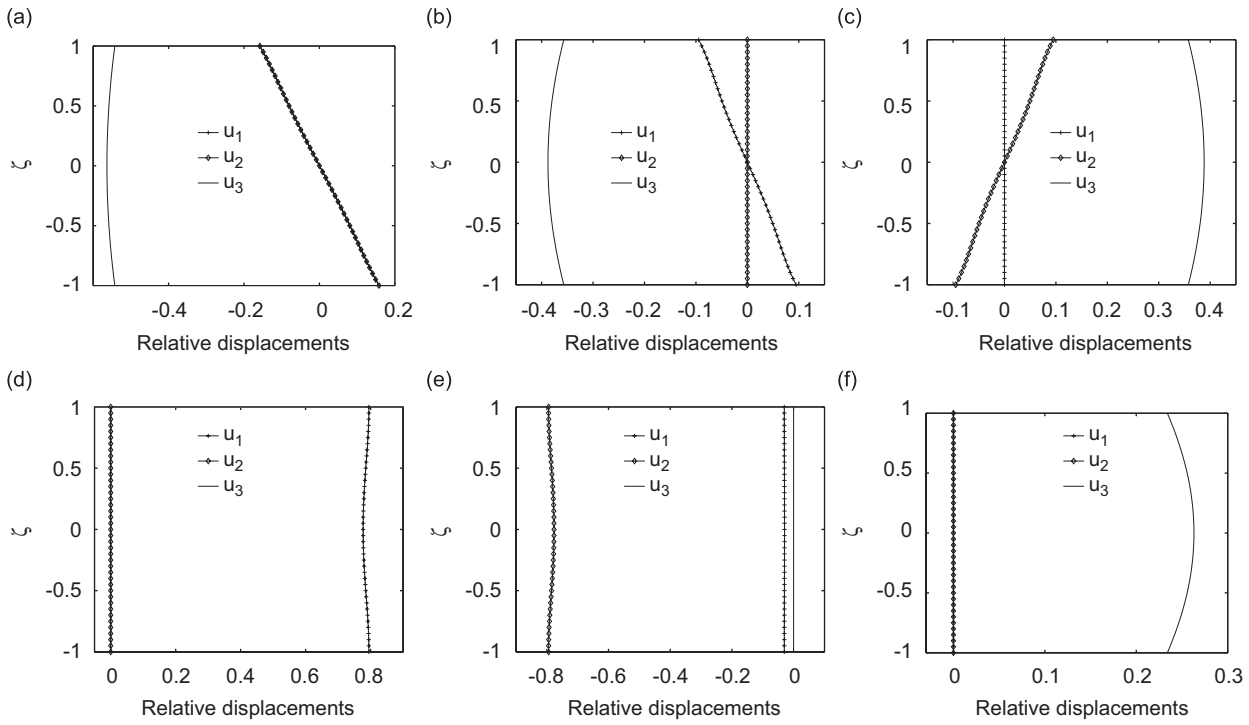

Fig. 6. Deflected shapes $U_i(0.5, 0.5, \zeta), i = 1, 2, 3$ of the first six modes for the square plates with four simply supported edges: (a) F_1, (b) F_2, (c) F_3, (d) TE_1, (e) TE_2 and (f) F_4.

solutions for thick plates because the three displacements of the plate are expanded by the triplicate summations of Chebyshev polynomials which can give better approximation to the variation of displacements in the thickness direction than the approximate 2-D plate theories. The power-law FGM sandwich plates with FGM facesheet and homogeneous core and the sandwich plates with homogeneous facesheet and FGM core are considered. The accuracy of the present approach is also validated by comparing the numerical results of isotropic and six types of power-law FGM sandwich plates with other theories. The convergence study reveals that the number of thickness expansion terms mainly depend on the thickness of the plate, and the length and width sides expansions mainly on the supported conditions. Moreover, the convergence rate is independent of κ value except for the unsymmetric distribution of material properties and very thick plates with clamped edges. Parametric study for layer thickness ratios, volume fraction indices, thickness-side and aspect ratios shows that the thin plates are slightly more sensitive to the material properties than the thick plates.

Acknowledgment

The authors would like to thank the Research Committee of University of Macau for its support.

Appendix A. Chebyshev polynomials

The Chebyshev polynomials of first 11 orders are listed below for reference:

$$P_1(x) = 1, \tag{A.1a}$$

$$P_2(x) = x, \tag{A.1b}$$

$$P_3(x) = 2x^2 - 1, \tag{A.1c}$$

$$P_4(x) = 4x^3 - 3x, \tag{A.1d}$$

$$P_5(x) = 8x^4 - 8x^2 + 1, \tag{A.1e}$$

$$P_6(x) = 16x^5 - 20x^3 + 5x, \tag{A.1f}$$

$$P_7(x) = 32x^6 - 48x^4 + 18x^2 - 1, \tag{A.1g}$$

$$P_8(x) = 64x^7 - 112x^5 + 56x^3 - 7x, \tag{A.1h}$$

$$P_9(x) = 128x^8 - 256x^6 + 160x^4 - 32x^2 + 1, \tag{A.1i}$$

$$P_{10}(x) = 256x^9 - 576x^7 + 432x^5 - 120x^3 + 9x, \tag{A.1j}$$

$$P_{11}(x) = 512x^{10} - 1280x^8 + 1120x^6 - 400x^4 + 50x^2 - 1. \tag{A.1k}$$

$$\vdots$$

Appendix B. Elements of submatrices

The elements of the nominal stiffness submatrices **K** and mass submatrices **M** are listed below:

$$\begin{aligned}\mathbf{K}_{11} = {} & p_1p_2\frac{bh}{a}K^{1,1}_{\xi,u_1iu_1\bar{i}}K^{0,0}_{\eta,u_1ju_1\bar{j}}E^{0,0}_{\zeta,k\bar{k}} + p_1\frac{bh}{a}K^{1,1}_{\xi,u_1iu_1\bar{i}}K^{0,0}_{\eta,u_1ju_1\bar{j}}E^{0,0}_{\zeta,k\bar{k}} \\ & + p_1\frac{ah}{2b}K^{0,0}_{\xi,u_1iu_1\bar{i}}K^{1,1}_{\eta,u_1ju_1\bar{j}}E^{0,0}_{\zeta,k\bar{k}} + p_1\frac{ab}{2h}K^{0,0}_{\xi,u_1iu_1\bar{i}}K^{0,0}_{\eta,u_1ju_1\bar{j}}E^{1,1}_{\zeta,k\bar{k}},\end{aligned} \tag{B.1a}$$

$$\mathbf{K}_{12} = p_1p_2hK^{1,0}_{\xi,u_1iu_2l}K^{0,1}_{\eta,u_1ju_2m}E^{0,0}_{\zeta,kn} + p_1\frac{h}{2}K^{0,1}_{\xi,u_1iu_2l}K^{1,0}_{\eta,u_1ju_2m}E^{0,0}_{\zeta,kn}, \tag{B.1b}$$

$$\mathbf{K}_{13} = p_1p_2bK^{1,0}_{\xi,u_1iu_3p}K^{0,0}_{\eta,u_1ju_3q}E^{0,1}_{\zeta,kr} + p_1\frac{b}{2}K^{0,1}_{\xi,u_1iu_3p}K^{0,0}_{\eta,u_1ju_3q}E^{1,0}_{\zeta,kr}, \tag{B.1c}$$

$$\begin{aligned}\mathbf{K}_{22} = {} & p_1p_2\frac{ah}{b}K^{0,0}_{\xi,u_2lu_2\bar{l}}K^{1,1}_{\eta,u_2mu_2\bar{m}}E^{0,0}_{\zeta,n\bar{n}} + p_1\frac{ah}{b}K^{0,0}_{\xi,u_2lu_2\bar{l}}K^{1,1}_{\eta,u_2mu_2\bar{m}}E^{0,0}_{\zeta,n\bar{n}} \\ & + p_1\frac{bh}{2a}K^{1,1}_{\xi,u_2lu_2\bar{l}}K^{0,0}_{\eta,u_2mu_2\bar{m}}E^{0,0}_{\zeta,n\bar{n}} + p_1\frac{ab}{2h}K^{0,0}_{\xi,u_2lu_2\bar{l}}K^{0,0}_{\eta,u_2mu_2\bar{m}}E^{1,1}_{\zeta,n\bar{n}},\end{aligned} \tag{B.1d}$$

$$\mathbf{K}_{23} = p_1p_2aK^{0,0}_{\xi,u_2lu_3p}K^{1,0}_{\eta,u_2mu_3q}E^{0,1}_{\zeta,nr} + p_1\frac{a}{2}K^{0,0}_{\xi,u_2lu_3p}K^{0,1}_{\eta,u_2mu_3q}E^{1,0}_{\zeta,nr}, \tag{B.1e}$$

$$\begin{aligned}\mathbf{K}_{33} = {} & p_1p_2\frac{ab}{h}K^{0,0}_{\xi,u_3pu_3\bar{p}}K^{0,0}_{\eta,u_3qu_3\bar{q}}E^{1,1}_{\zeta,r\bar{r}} + p_1\frac{ab}{h}K^{0,0}_{\xi,u_3pu_3\bar{p}}K^{0,0}_{\eta,u_3qu_3\bar{q}}E^{1,1}_{\zeta,r\bar{r}} \\ & + p_1\frac{bh}{2a}K^{1,1}_{\xi,u_3pu_3\bar{p}}K^{0,0}_{\eta,u_3qu_3\bar{q}}E^{0,0}_{\zeta,r\bar{r}} + p_1\frac{ah}{2b}K^{0,0}_{\xi,u_3pu_3\bar{p}}K^{1,1}_{\eta,u_3qu_3\bar{q}}E^{0,0}_{\zeta,r\bar{r}},\end{aligned} \tag{B.1f}$$

$$\mathbf{M}_{11} = \frac{abh}{8}K^{0,0}_{\xi,u_1iu_1\bar{i}}K^{0,0}_{\eta,u_1ju_1\bar{j}}M_{\zeta,k\bar{k}}, \tag{B.2a}$$

$$\mathbf{M}_{22} = \frac{abh}{8}K^{0,0}_{\xi,u_2lu_2\bar{l}}K^{0,0}_{\eta,u_2mu_2\bar{m}}M_{\zeta,n\bar{n}}, \tag{B.2b}$$

$$\mathbf{M}_{33} = \frac{abh}{8}K^{0,0}_{\xi,u_3pu_3\bar{p}}K^{0,0}_{\eta,u_3qu_3\bar{q}}M_{\zeta,r\bar{r}}, \tag{B.2c}$$

where $p_1 = 1/[2(1+v)]$, $p_2 = v/(1-2v)$ are the constants related to Poisson's ratio.

For the describable convenience, the operators K_ξ, K_η, E_ζ and M_ζ are used in above equations and they are defined as

$$K^{s,\bar{s}}_{\xi,\sigma\varphi\bar{\sigma}\bar{\varphi}} = \int_{-1}^{1} \frac{\mathrm{d}^s[f^{(1)}_\sigma(\xi)P_\varphi(\xi)]}{\mathrm{d}\xi^s} \cdot \frac{\mathrm{d}^{\bar{s}}[f^{(1)}_{\bar{\sigma}}(\xi)P_{\bar{\varphi}}(\xi)]}{\mathrm{d}\xi^{\bar{s}}}\,\mathrm{d}\xi, \tag{B.3a}$$

$$K^{s,\bar{s}}_{\eta,\sigma\varphi\bar{\sigma}\bar{\varphi}} = \int_{-1}^{1} \frac{\mathrm{d}^s[f^{(2)}_\sigma(\eta)P_\varphi(\eta)]}{\mathrm{d}\eta^s} \cdot \frac{\mathrm{d}^{\bar{s}}[f^{(2)}_{\bar{\sigma}}(\eta)P_{\bar{\varphi}}(\eta)]}{\mathrm{d}\eta^{\bar{s}}}\,\mathrm{d}\eta, \tag{B.3b}$$

$$E^{s,\bar{s}}_{\zeta,\varphi\bar{\varphi}} = \sum_{i=1}^{N_L} \int_{\zeta_i}^{\zeta_{i+1}} E_i(\zeta) \cdot \frac{\mathrm{d}^s P_\varphi(\zeta)}{\mathrm{d}\zeta^s} \cdot \frac{\mathrm{d}^{\bar{s}} P_{\bar{\varphi}}(\zeta)}{\mathrm{d}\zeta^{\bar{s}}}\,\mathrm{d}\zeta, \tag{B.3c}$$

$$M_{\zeta,\varphi\bar{\varphi}} = \sum_{i=1}^{N_L} \int_{\zeta_i}^{\zeta_{i+1}} \rho_i(\zeta) \cdot P_\varphi(\zeta)P_{\bar{\varphi}}(\zeta)\,\mathrm{d}\zeta, \tag{B.3d}$$

where

$$s, \bar{s} = 0, 1,$$

$$\sigma, \bar{\sigma} = u_1, u_2, u_3,$$

$$\varphi, \bar{\varphi} = i, \bar{i}, j, \bar{j}, k, \bar{k}, l, \bar{l}, m, \bar{m}, n, \bar{n}, p, \bar{p}, q, \bar{q}, r, \bar{r}. \tag{B.4}$$

N_L is the number of layers; $E_i(\zeta)$ in Eq. (B.3c) and $\rho_i(\zeta)$ in Eq. (B.3d) are the thickness-graded Young's modulus and mass density of the FGM plate.

References

[1] M. Yamanouchi, M. Koizumi, T. Hirai, I. Shiota, *Proceedings of First International Symposium on Functionally Gradient Materials*, Sendai, Japan, 1990.

[2] M. Koizumi, The concept of FGM, *Ceramic Transactions. Functionally Gradient Materials* 34 (1993) 3–10.

[3] G. Bao, L. Wang, Multiple cracking in functionally graded ceramic/metal coatings, *International Journal of Solids and Structures* 32 (1995) 2853–2871.

[4] P.R. Marur, Fracture Behaviour of Functionally Graded Materials, PhD Thesis, Auburn University, Alabama, 1999.

[5] [a] R.L. Williamson, B.H. Rabin, J.T. Drake, Finite element analysis of thermal residual stresses at graded ceramic–metal interfaces—part I: model description and geometrical effects, *Journal of Applied Physics* 74 (1993) 1310–1320;
[b] J.T. Drake, R.L. Williamson, B.H. Rabin, Finite element analysis of thermal residual stresses at graded ceramic–metal interfaces—part II: interface optimization for residual stress reduction, *Journal of Applied Physics* 74 (1993) 1321–1326.

[6] Naotake Noda, Thermal stresses in functionally graded materials, *Journal of Thermal Stresses* 22 (1999) 477–512.

[7] O. Kesler, M. Finot, S. Sampath, Determination of processing-induced stresses and properties of layered and graded coatings: experimental method and results for plasma-sprayed Ni-Al_2O_3, *Acta Materialia* 45 (1997) 3123–3134.

[8] P. Kwon, M. Crimp, Automating the design process and powder processing of functionally gradient materials, *Composites and Functionally Graded Materials* 80 (1997) 73–88.

[9] J.N. Reddy, Analysis of functionally graded plates, *International Journal for Numerical Methods in Engineering* 47 (2000) 663–684.

[10] Z.Q. Cheng, R.C. Batra, Exact correspondence between eigenvalues of membranes and functionally graded simply supported polygonal plates, *Journal of Sound and Vibration* 229 (2000) 879–895.

[11] C.T. Loy, K.Y. Lam, J.N. Reddy, Vibration of functionally graded cylindrical shells, *International Journal of Mechanical Sciences* 41 (1999) 309–324.

[12] G.V. Praveen, J.N. Reddy, Nonlinear transient thermoelastic analysis of functionally graded ceramic–metal plates, *International Journal of Solids and Structures* 35 (1998) 4457–4476.

[13] J.N. Reddy, Z.Q. Cheng, Three-dimensional solutions of smart functionally graded plates, *Journal of Applied Mechanics* 68 (2001) 234–241.

[14] S.S. Vel, R.C. Batra, Three-dimensional exact solution for the vibration of functionally graded rectangular plates, *Journal of Sound and Vibration* 272 (2004) 703–730.

[15] S. Venkataraman, B.V. Sankar, Analysis of sandwich beams with functionally graded core, *Proceedings of the 42nd AIAA/ASME/ASCE/AHS/ASC Structures, Structural Dynamics, and Materials Conference*, AIAA-2001-1281, Seattle, 2001, 16–19 April 2001.

[16] T.A. Anderson, A 3-D elasticity solution for a sandwich composite with functionally graded core subjected to transverse loading by a rigid sphere, *Composite Structures* 60 (2003) 265–274.

[17] E. Pan, F. Han, Exact solution for functionally graded and layered magneto-electro-elastic plates, *International Journal of Engineering Science* 43 (2005) 321–339.
[18] M. Das, A. Barut, E. Madenci, D.R. Ambur, A triangular plate element for thermo-elastic analysis of sandwich panels with a functionally graded core, *International Journal for Numerical Method in Engineering* 68 (2006) 940–966.
[19] H.S. Shen, Postbuckling of FGM plates with piezoelectric actuators under thermo-electro-mechanical loadings, *International Journal of Solids and Structures* 42 (2005) 6101–6121.
[20] N. Noda, Thermal stress in functionally graded materials, *Third International Congress on Thermal Stresses*, *Thermal Stresses '99*, Cracow, Poland, 13–17 June 1999.
[21] [a] A.M. Zenkour, A comprehensive analysis of functionally graded sandwich plates: part 1—deflection and stresses, *International Journal of Solids and Structures* 42 (2005) 5224–5242;
[b] A.M. Zenkour, A comprehensive analysis of functionally graded sandwich plates: part 2—buckling and free vibration, *International Journal of Solids and Structures* 42 (2005) 5243–5258.
[22] Y.K. Cheung, D. Zhou, Three-dimensional vibration analysis of cantilevered and completely free isosceles triangular plates, *International Journal of Solids and Structures* 39 (2002) 673–687.
[23] D. Zhou, Y.K. Cheung, F.T.K. Au, S.H. Lo, Three-dimensional vibration analysis of thick rectangular plates using Chebyshev polynomials and Ritz method, *International Journal of Solids and Structures* 39 (2002) 6339–6353.
[24] Y.Y. Yung, D. Munz, Stress analysis in a two materials joint with a functionally graded materials, *Functionally Graded Material* (1996) 41–46.
[25] Z.H. Jin, G.H. Paulino, Transient thermal stress analysis of an edge crack in a functionally graded material, *International Journal of Fracture* 107 (2001) 73–98.
[26] F. Delale, F. Erdogan, The crack problem for a nonhomogeneous plane, *Journal of Applied Mechanics* 50 (1983) 609–614.
[27] L. Fox, I.B. Parker, *Chebyshev Polynomials in Numerical Analysis*, Oxford University Press, London, 1968.
[28] V.L. Rvachev, T.I. Sheiko, R-functions in boundary value problems in mechanics, *Applied Mechanics Review* 48 (4) (1995) 151–187.
[29] Q. Li, V.P. Iu, K.P. Kou, Three-dimensional vibration analysis of functionally graded material rectangular plates by Chebyshev polynomials, *Proceedings of the Tenth International Conference on Enhancement and Promotion of Computational Methods in Engineering and Science*, Sanya, China, August 2006.
[30] M. Malik, C.W. Bert, Three-dimensional elasticity solutions for free vibrations of rectangular plates by the differential quadrature method, *International Journal of Solids and Structures* 35 (1998) 299–318.